Universiteit Antwerpen

This item is the archived peer-reviewed author-version of:

A spectral mixing model accounting for multiple reflections and shadow

Reference:
Andrejchenko Vera, Zahiri Zohreh, Heylen Rob, Scheunders Paul.- A spectral mixing model accounting for multiple reflections and shadow
Proceedings of IGARSS 2019, International Geoscience and Remote Sensing Symposium, Yokohama, July 28-August 2, 2019 - ISSN 2153-7003 - Yokohama, Japan, IEEE, 2019, p. 286-289
Full text (Publisher's DOI): https://doi.org/10.1109/IGARSS.2019.8897856

uantwerpen.be
Institutional repository IRUA

A SPECTRAL MIXING MODEL ACCOUNTING FOR MULTIPLE REFLECTIONS AND SHADOW

Vera Andrejchenko, Zohreh Zahiri, Rob Heylen, Paul Scheunders

Imec-Visionlab, University of Antwerp

ABSTRACT

In this work, we present a nonlinear spectral mixing model that, apart from the fractional abundances, contains two additional parameters, one accounting for multiple reflections and another accounting for shadow. The model is based on the multilinear mixing (MLM) model that we have proposed earlier. An analysis of the parameter values is performed on a close-range hyperspectral image of a building facade. The model is compared to the linear model and two models that account for only one of the two effects: the linear model with an extra shadow endmember, and the MLM model.

Index Terms— hyperspectral unxming, multiple reflections, shadows

1. INTRODUCTION

Hyperspectral unmixing aims to decompose each observed pixel spectrum into a number of pure component spectra, i.e. endmembers. The linear mixing model (LMM) assumes that each spectrum is a linear combination or pure materials, where the linear coefficients denote their fractional abundances within the pixel. Often, these abundances are assumed to be non-negative, leading to the abundance nonnegativity constraint(ANC). When the entire spectral signal is decomposed into endmember contributions, the abundances sum up to one, leading to the sum-to-one constraint (ASC). This particular model allows a light ray to interact with a single material (endmember) before reaching the sensor. Moreover, it assumes flat surfaces with nicely segregated endmember materials. It was proven to work in certain scenarios [1].

However, in real life scenarios, the linear model is not entirely adequate. Phenomena such as multiple scattering, shadows, spatial neighborhood effects etc. contribute to a nonlinear behavior of the material mixtures. To accomodate this, models allowing light to interact with 2 endmember materials i.e. secondary reflections were developed, such as the bilinear unmixing models [2–5]. Theoretically, the bilinear models can be extended to higher order interactions, but they are often not physically based and become hard to solve.

Recently, we have developed a multilinear mixing model (MLM), a model that takes multiple reflections into account [6]. MLM includes all higher order interactions by introducing one single parameter that describes the probability that a light ray undergoes a further interaction after each interaction with a material. This model is analytically tractable and physically sound and useful in practical situations where nonlinearities due to multiple reflections are apparent.

So far, most nonlinear unmixing methods were validated in Earth observation settings, either on synthetic data or well known hyperspectral remote sensing images. One problem with hyperspectral remote sensing images is their limited spatial resolution. Subtle nonlinear effects typically take place on a scale, smaller than the pixel size, and are expected to average out, making the linear contribution the dominant one. In this work, we investigate nonlinear spectral unmixing in a close-range setting. Images of high spatial resolution are expected to reveal subtle nonlinear effects. One particular effect that reveals nonlinear behavior is shadow. Since shadowed areas do not receive direct light, all light reaching the sensor from shadowed areas have a nonlinear origin. It is therefore important to properly describe shadow in a nonlinear spectral mixing model.

In this work, we included a shadow parameter in the MLM model. This allows to identify shadowed areas, and to study the reflectance from such areas. The model will be validated on a high-resolution close-range hyperspectral image of a building facade.

2. METHOD

2.1. The MLM model

The MLM model [6] allows the light to interact multiple times with materials. It is based on a ray-based approximation of light, tracing the path of a single light ray from the source to the observer. This path can be modeled as a Markov chain following certain rules:

- An incoming light ray interacts with at least one material.
- After each interaction with a material, the ray has a probability P of undergoing further interactions, and a probability $(1 - P)$ of escaping the scene and reaching the observer.

- The probability of interacting with material i is proportional to its abundance a_i.

- When a light ray is scattered by material i, its intensity changes according to that materials reflectance $\boldsymbol{e}_i$.

The resulting mixing equation then becomes:

$$\begin{aligned}\boldsymbol{x} &= (1-P)\sum_{i=1}^{p} a_i\boldsymbol{e}_i + (1-P)P\sum_{i=1}^{p}\sum_{j=1}^{p} a_i a_j \boldsymbol{e}_i \odot \boldsymbol{e}_j \\ &\quad +(1-P)P^2\sum_{i=1}^{p}\sum_{j=1}^{p}\sum_{k=1}^{p} a_i a_j a_k \boldsymbol{e}_i \odot \boldsymbol{e}_j \odot \boldsymbol{e}_k \ldots \\ &= \frac{(1-P)\sum_{i=1}^{p} a_i\boldsymbol{e}_i}{1-P\sum_{i=1}^{p} a_i\boldsymbol{e}_i} \end{aligned} \quad (1)$$

The MLM model accommodates all orders of interactions between endmembers, and scales all higher-order interactions with a single parameter P with a clear physical interpretation (the probability of interacting again with an endmember). We refer to [6] for more details.

2.2. A shadow MLM model (SMLM)

In this section, we extend the MLM model with the capability of dealing with shadows, resulting in the shadow MLM (SMLM) model. Shadows play an important role in the composition of a scene. These shadows may be partial, when only part of the IFOV of a pixel is be shadowed, or when the object that casts the shadow is smaller than the IFOV (e.g. small trees and bushes). By definition, any object that is shadowed has no direct line of sight to the light source. When we consider the MLM model and its series expansion, this means that in shadowed regions only interactions of order two and higher are allowed, while directly illuminated parts of the pixel also have contributions from the first-order interactions. By introducing a parameter $Q \in [0,1]$ where $Q = 0$ means no shadow, while $Q = 1$ indicates a full shadow situation, the following mixing equation for the SMLM model is obtained:

$$\boldsymbol{x} = \frac{(1-P)\sum_{i=1}^{p} a_i\boldsymbol{e}_i}{1-P\sum_{i=1}^{p} a_i\boldsymbol{e}_i} - Q(1-P)\sum_{i=1}^{p} a_i\boldsymbol{e}_i \quad (2)$$

Both models, MLM and SMLM can be inverted to obtain the fractional abundances from the reflectance. For this, we performed constrained optimization of the reconstruction error versus the model parameters via sequential quadratic programming. The model parameters P in the case of MLM and both P and Q in the case of SMLM are estimated along with the fractional abundances and a map of these parameters reveals additional information on the spatial location of regions where multiple reflections occur and on shadowed regions.

3. EXPERIMENTS AND RESULTS

A a preliminary study, the parameters of the SMLM model were evaluated on a real close-range hyperspectral image, taken from a selected historic building facade in Bergen (Norway). The south view of the building was scanned with a Hyspex 320m hyperspectral camera (Norks Elektro Optikk AS, Oslo, Norway) from an offset of almost 15 m to the facade. The camera has a spectral range in the shortwave infrared (1,300-2,500 nm), with a spectral resolution of 5nm. A number of preprocessing steps such as dark image subtraction, linear interpolation of bad pixels, non-uniformity corrections, relative reflection calibration and MNF denoising were performed (see [7] for more details).

Ground-truth was manually obtained for five different materials: brick, mortar, rendering, stone and painted window frame. Endmembers were obtained as average spectra of the ground-truth data for the different materials. Since glass has very low reflectance values and can easily be mixed up with shadow and/or multiple reflections, no endmember for glass was defined.

The proposed SMLM model was applied to this image. We made a comparison with 3 alternatives:

- The linear mixing model (LMM), with ANC and ASC imposed on the abundances [1]. The mixing model is given by:

$$\boldsymbol{x} = \sum_{i=1}^{p} a_i\boldsymbol{e}_i, \quad \begin{cases}\sum_i a_i = 1 \\ \forall i : a_i \geq 0\end{cases} \quad (3)$$

- SLMM: LMM with an extension of the endmember matrix with an aditional zero-vector shadow endmember:

$$\begin{aligned}\boldsymbol{x} &= (1-Q)\sum_{i=1}^{p} a_i\boldsymbol{e}_i, \quad \begin{cases}\sum_i a_i = 1 \\ \forall i : a_i \geq 0 \\ Q \in [0,1]\end{cases} \\ &= \sum_{i=1}^{p} \hat{a}_i\boldsymbol{e}_i + \hat{a}_{p+1}\overline{0}, \quad \begin{cases}\sum_{i=1}^{p+1} \hat{a}_i = 1 \\ \forall i : \hat{a}_i \geq 0\end{cases} \\ &\quad \text{with} \quad \begin{cases}\forall i \in 1,\ldots,p : \hat{a}_i = (1-Q)a_i \\ \hat{a}_{p+1} = Q = 1 - \sum_{i=1}^{p} \hat{a}_i\end{cases}\end{aligned} \quad (4)$$

- The MLM model [6], given by (1).

Note that the $P \to 0$ limit of the SMLM model equals the SLMM model, the $Q \to 0$ limit gives the MLM model, and the $P, Q \to 0$ limit gives the LMM model.

For LMM and SLMM we employed the fully-constrained least-squares unmixing (FCLSU) algorithm [1], based on the nonnegatively-constrained least-squares algorithm by Lawson and Hanson [8].

The obtained maps of the model parameters are shown in Fig. 1. Moreover, scatter plots between the parameters of the different models can be seen in Fig.2. Abundance maps [1] were calculated and compared to classification maps obtained by using the ground truth data as training data in a SVM classifier.

The following observations can be made from these figures:

- From both the parameter maps and the scatterplot, it can be observed that the shadow abundance map of SLMM and the P map of MLM are very similar, indicating that the effect of these parameters are similar in both models. This can be attributed to the fact that the first order term from the series expansion of the MLM model (Eq. 1) corresponds to the SLMM model.
- Wherever the P value of MLM and the shadow abundance of SLMM differs from zero, one or both of the parameters of SMLM differ from zero. The P values of SMLM are always equal to or lower than the ones of MLM, while the Q values of SMLM are always equal to or lower than the shadow abundance values of SLMM (except for the values close to 1).
- The windows show high values for the SMLM parameters. While SLMM regards these areas as shadow and MLM regards them as areas of multiple reflections, the SMLM model seems to divide the effect over both parameters, with an emphasis on the parameter P.
- Shadowed areas, e.g. under the stone sills on top and beneath the windows, also have high parameter values. Again SLMM regards these areas as shadow and MLM as areas of multiple reflections. SMLM there shows high shadow values (high Q). The shadowed regions above and under glass areas seem to indicate more multiple reflections (high P) than the shadowed areas above or under the window frames.
- Analysis of the obtained abundance maps learns that the LMM model deviates most from the classification maps. The abundance values of SLMM are in general lower than the abundance values of MLM and SMLM. This is in particular the case when the shadow abundance is high. Differences between abundance maps of MLM and SMLM are very small.
- In shadowed regions (e.g. under the stone sills beneath the windows), SMLM and MLM show high abundance values for brick. Since in shadowed regions no linear but only higher order reflections appear, this shows that these models are able to reveal fractional abundance information of materials under the shadow. SLMM is able to determine these shadowed areas but shows reduced abundance values for all materials.

[1] All abundance maps

4. CONCLUSIONS

In this work, we have presented an extension of a nonlinear mixing model, by including shadow and multiple reflections. As a preliminar validation of these effects, the model parameter were evaluated by an experiment on a close range hyperspectral image in the SWIR of a building facade. In the future, we want to further validate the SMLM model for its ability to estimate fractional abundances, in particular in shadowed regions, where only higher order reflections appear.

5. REFERENCES

[1] D.C. Heinz and C.-I Chang, "Fully constrained least squares linear spectral mixture analysis method for material quantification in hyperspectral imagery," *IEEE Trans. Geosci. Remote Sens.*, vol. 39, no. 3, pp. 529–545, 2001.

[2] J.M.P. Nascimento and J.M. Bioucas-Dias, "Nonlinear mixture model for hyperspectral unmixing," *Image Sig. Process. for Remote Sens. XV*, vol. 7477, no. 1, pp. 74770I, 2009.

[3] B. Somers, K. Cools, S. Delalieux, J. Stuckens, D. Van der Zande, W.W. Verstraeten, and P. Coppin, "Nonlinear hyperspectral image analysis for tree cover estimates in orchards," *Remote Sens. Environ.*, vol. 113, pp. 1183–1193, 2009.

[4] W. Fan, B. Hu, J. Miller, and M. Li, "Comparative study between a new nonlinear model and common linear model for analysing laboratory simulated forest hyperspectral data," *Int. J. Remote Sens.*, vol. 30, no. 11, pp. 2951–2962, 2009.

[5] A. Halimi, Y. Altmann, N. Dobigeon, and J.-Y. Tourneret, "Nonlinear unmixing of hyperspectral images using a generalized bilinear model," *IEEE Trans. Geosci. Remote Sens.*, vol. 49, no. 11, pp. 4153–4162, 2011.

[6] R. Heylen and P. Scheunders, "A multilinear mixing model for nonlinear spectral unmixing," *IEEE Trans. Geosci. Remote Sens.*, vol. 54, no. 1, pp. 240–251, 2016.

[7] Tobias Kurz, Simon Buckley, and John Howell, "Close-range hyperspectral imaging for geological field studies: workflow and methods," *Int. J. of Remote Sens.*, vol. 34, no. 5, pp. 1798–1822, 2013.

[8] C.L. Lawson and R.J. Hanson, *Solving Least Squares Problems*, Prentice Hall, Englewood Cliffs, NJ, 1974.

RGB image

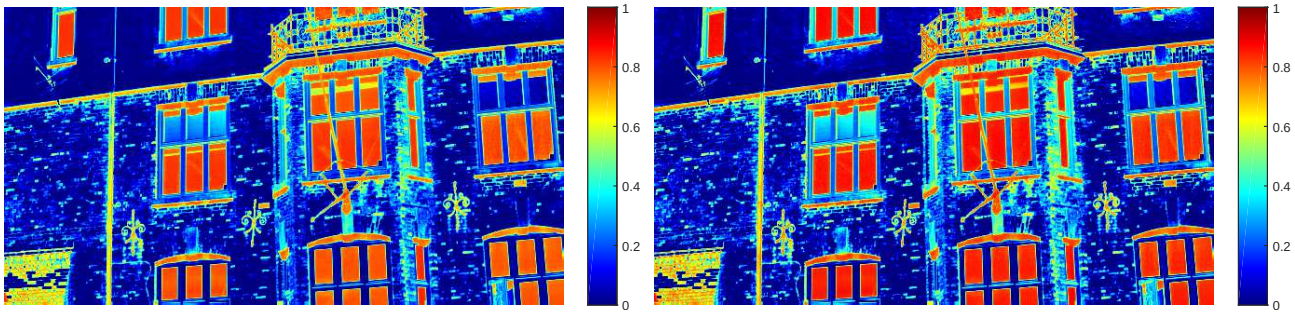

SLMM shadow MLM P

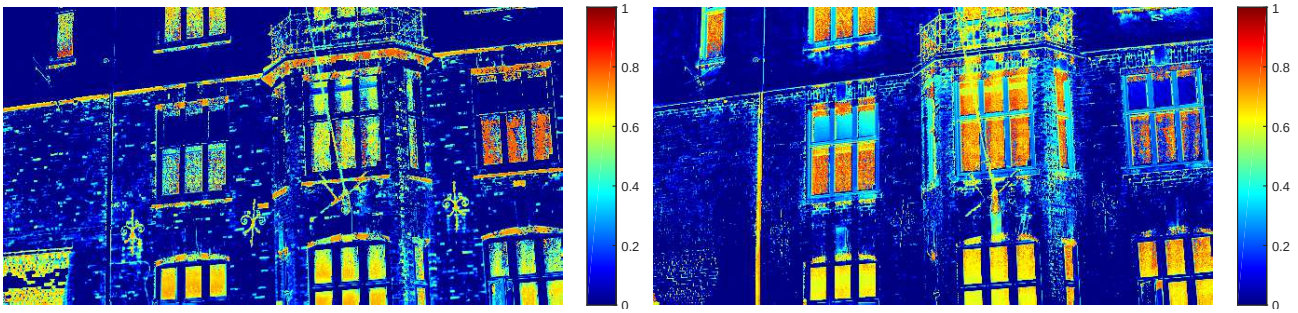

SMLM Q SMLM P

Fig. 1. RGB image, the shadow abundance map from the SLMM model, the P map from the MLM model and the Q and P maps from the SMLM model.

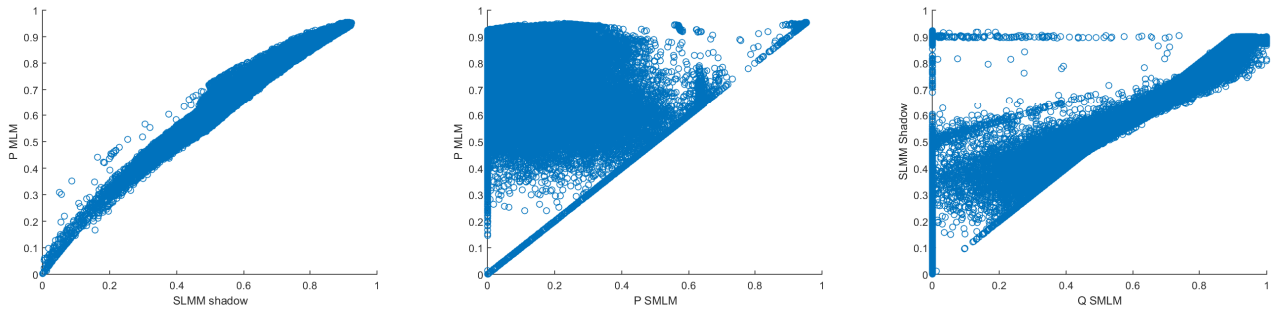

a b c

Fig. 2. Scatterplots between the model parameters of the different models, obtained from the building image; a) the shadow abundance values of SLMM versus the P values of MLM; b) the P values of SMLM versus the P values of MLM; c) the Q values of SMLM versus the shadow abundance values of SLMM;